

MC²-3/TWODANT/DIF3D Analysis for the ZPPR-15 ¹⁰B(n, α) Reaction Rate Measurement

Min Jae Lee^{a*}, Donny Hartanto^a, Sang Ji Kim^a, and Changho Lee^b

^aKorea Atomic Energy Research Institute (KAERI)

989-111 Daedeok-daero, Yuseong-gu, Daejeon 305-353, Republic of Korea

^bArgonne National Laboratory (ANL)

9700 S. Cass Ave, Argonne IL 60439, USA

*Corresponding author: lmj@kaeri.re.kr

Abstract – As a validation procedure of the fast reactor core neutronics design code system of Prototype Gen-IV Sodium-cooled Fast Reactor (PGSFR), ZPPR-15 ¹⁰B(n, α) reaction rate measurement were modeled and analyzed by MC²-3/TWODANT/DIF3D-VARIANT. In order to provide a reliable reference solution, a weight window technique was applied to MCNP calculation for estimating the neutron flux and reaction rate at each detection point. The reaction rate for 6 different positions at outer core, Boron-Carbide / Sodium (BCNA) shield, Stainless Steel / Sodium (SSNA) shield, and Sodium Pool (SP) were estimated and normalized by the value at outer-core. The error of estimated value tends to be increased from BCNA to SP as the measured position becomes far away from the core center, and the maximum error was observed at SP as about 20%, but the difference between deterministic and Monte Carlo results was minor. By comparing the spectrum and reaction rate distribution over the energy grid, the deterministic results can be considered generally reliable compared to Monte Carlo results, but considerable discrepancies were observed around the resonances of Na-23 and Fe-56.

I. INTRODUCTION

Zero Power Physics Reactor-15 (ZPPR-15) is a mock-up experiment of Integral Fast Reactor (IFR) program, which was performed in USA [1]. Among integral physics experiments performed in ZPPR-15, B-10 reaction rate measurements are analyzed in this work by MC²-3 [2] and DIF3D-VARIANT [3] as a validation procedure of the fast reactor core neutronics design code system of Prototype Gen-IV Sodium-cooled Fast Reactor (PGSFR) [4].

B-10 reaction rate measurement was performed in ZPPR-15 phase B, in which the fuel material was Pu-U-Mo alloy. The core configuration for B-10 reaction rate measurement is plotted in Fig. 1. In the figure, SP, BCNA, and SSNA stand for sodium pool, boron carbide/sodium configuration, and stainless steel/sodium configuration respectively. In the experiment, ¹⁰B(n, α) reaction rate is measured by the gas proportional counter from outer core to sodium pool at 6 different radial positions as indicated in Fig. 1. Loading numbers 127 to 132 are assigned based on the detector position from sodium pool to outer core.

Since relative absorption rates were measured in this experiments, additional information, such as neutron spectrum and reaction rate distribution over the multi-group energy grid, was estimated by as-built Monte Carlo Models. The relative ¹⁰B(n, α) reaction rate was compared to both measured and Monte Carlo values, while others were verified with Monte Carlo results in this manuscript.

II. DEVELOPMENT OF DETERMINISTIC MODELS

The calculation procedure of the MC²-3/TWODANT/DIF3D-VARIANT code system for the ZPPR-15 ¹⁰B(n, α)

reaction rate analysis is shown in Fig. 2. The first step is generating 1041G homogenized cross section for TWODANT R-Z calculation. Second, TWODANT eigenvalue calculation is performed to obtain region-wise neutron spectrum which will be utilized for group collapsing. Even though TWODANT is based on Sn transport method, the calculation does not take long computing time since the R-Z model is simplified one and the mesh grid is coarse. A 33G homogenized cross section library is generated in the next MC²-3 runs. Finally, DIF3D-VARIANT calculations are performed to estimate the k-eff as well as the flux distribution.

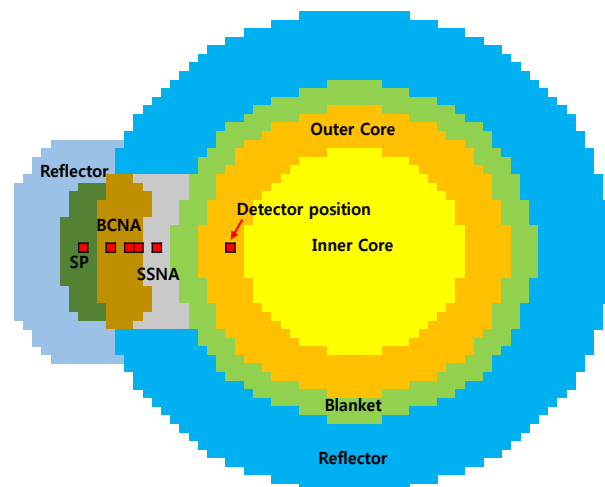


Fig. 1. Radial core layout of ZPPR-15B core

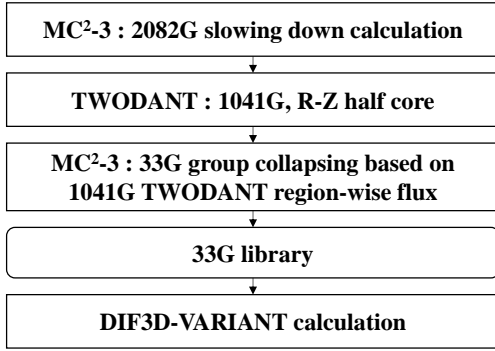


Fig. 2. MC²-3/TWODANT/DIF3D-VARIANT calculation procedure

During the MC²-3 calculation, a 1D transport calculation was performed to consider the heterogeneity effects for fuel drawers. The drawer, which is equivalent to an assembly in a power reactor, is heterogeneous in 3D as plotted in Fig. 3, so it is not straight-forward to convert the real geometry into 1D slab models. However, the geometry is less complex and heterogeneous in y and z directions as plotted in Fig. 4, the slab geometry can be developed along the x-directional material regions. However, there are remained structures in y- and z-directions. One can put those materials on the both boundary of x-axis by preserving volume fraction of each regions as focused regions in Fig 5. In this manner, the background effect of surrounding materials on y- and z- direction can be taken into account during the slowing down calculation.

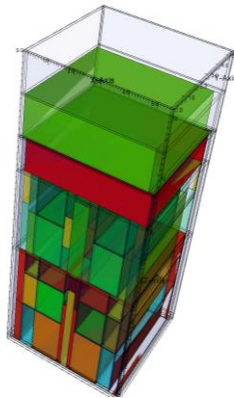


Fig. 3. A sample image of ZPPR-15 fuel drawer (axially re-scaled)

The MC²-3 0D slowing down calculation was performed to others including blanket, shielding and reflector regions. In this case, the realistic neutron spectrum can be reflected during the group collapsing procedure, by adopting the neutron spectrum for TWODANT R-Z calculation. The boron deposit in the counter was sufficiently thin, so the boron cross section for ¹⁰B(n, α) reaction rate can be generated with infinite dilute conditions.

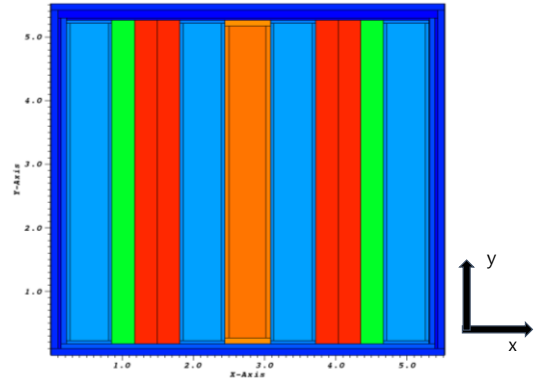


Fig. 4. X-Y cross-sectional view of a fuel drawer

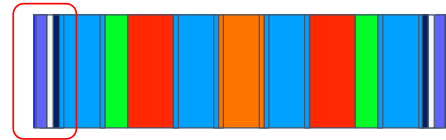


Fig. 5. A 1D slab model for MC²-3 1D CPM calculation

Because of the shielding area, the core is not symmetric and an equivalent R-Z models can be hardly made. In order to overcome this, two TWODANT models are developed separately; one is a R-Z model with typical reflector ignoring the shielding area, and another is a R-Z model surrounded by the shielding attached on the left side without typical radial reflector in Fig. 1. The cross sections of shielding regions are generated based on the neutron spectrum for the second model, and others are generated based on the first model.

III. REFERENCE MCNP CALCULATION

Achieving small uncertainties for local tallies near problem boundary is harsh for Monte Carlo criticality calculation due to low population of neutrons. The uncertainty can be only reduced inversely proportional to the squared-root of histories, and the accuracy is limited by computing resources. Unlike criticality problems, the uncertainty can be easily reduced by weight window technique for fixed source problems. Recently, MCNP 6.0 provides a procedure to convert eigenvalue problem to fixed source problem by tracking all the fission locations that can be banked during a criticality calculation [6]. Two MCNP runs are required: the first one for finding fission locations, and the second run for shielding calculation with predefined fission sources. The uncertainty of reaction rates can be drastically reduced especially for the tallies in sodium pool by applying weight window technique.

IV. CALCULATION RESULT AND DISCUSSIONS

1. Estimation of relative $^{10}\text{B}(n,\alpha)$ absorption rate

The calculation results of both Monte Carlo and deterministic models are summarized in Tables I and II compared to the measured values. Note that the MCNP-A, and MCNP-B in Tables I and II represent the MCNP with weight window, and conventional eigenvalue calculation in MCNP respectively, and deterministic results are denoted as DIF3D for convenience. 5 million histories and 1 billion histories are used to obtain MCNP-A and MCNP-B results respectively. Before directly comparing the estimated reaction rates to measured ones, the improved MCNP solution can be found in Table I. The standard deviation of $^{10}\text{B}(n,\alpha)$ of MCNP-A is only 0.72% for sodium pool, while it is about 11% for conventional MCNP results. 200 times less number of histories were simulated in MCNP-A, but better results could be achieved.

Figs. 6 and 7 show the reaction rate and error at each detector location. Between two MCNP results, MCNP-A results are used for comparisons hereafter. The relative reaction rate for both MCNP and DIF3D show good agreement with the measured values as plotted in Fig. 3. The error trends seem to be increased when the detector location becomes close to sodium pool, as it was 5% for SSNA, 5~15% for BCNA and 20% for SP. The error plotted in Fig. 4 shows similar trends for both MCNP and DIF3D.

Additionally, the neutron flux level at each location is compared in Fig. 5 between MCNP and DIF3D although the

total flux was not measured in the experiment. The flux level in DIF3D is very similar to MCNP results with 3% difference maximally. From the comparison of reaction rate and total flux, the DIF3D results can be considered quite consistent with MCNP's as well as the measurements.

2. Comparisons of neutron spectrum and reaction rate

The neutron spectrum and reaction rate at each energy group were calculated to confirm the agreement between DIF3D and MCNP results. From Fig 9 to Fig 12 show the neutron spectrum and reaction rate calculated for six different locations in SP, BCNA, SSNA and outer core.

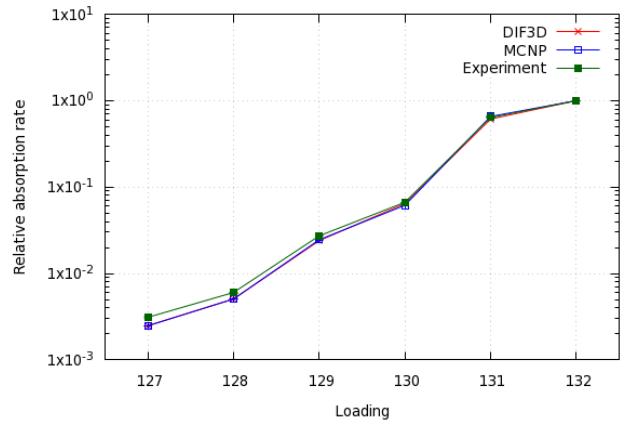


Fig. 6. Relative $^{10}\text{B}(n,\alpha)$ reaction rate

Table I. Relative $^{10}\text{B}(n,\alpha)$ absorption rate

Loading	Region	Measured		MCNP-A		MCNP-B		MC ² -3/DIF3D
		$^{10}\text{B}(n,\alpha)$	σ, rel	$^{10}\text{B}(n,\alpha)$	σ, rel	$^{10}\text{B}(n,\alpha)$	σ, rel	$^{10}\text{B}(n,\alpha)$
127	SP	0.0311	0.0225	0.0248	0.0072	0.0263	0.1081	0.0249
128	SH(BCNA)	0.0603	0.0133	0.0507	0.0064	0.0544	0.0385	0.0507
129	SH(BCNA)	0.2730	0.0070	0.2461	0.0068	0.2621	0.0184	0.2402
130	SH(BCNA)	0.6660	0.0041	0.6150	0.0098	0.6572	0.0144	0.6447
131	RR(SSNA)	6.3820	0.0020	6.4168	0.0097	6.0590	0.0125	6.1245
132	OC	10.0000	0.0100	10.0000	0.0051	10.0000	0.0027	10.0000

Table II. C/E values for $^{10}\text{B}(n,\alpha)$ absorption rate

Loading	Region	MCNP-A		MCNP-B		MC ² -3/DIF3D	
		C/E	σ, rel	C/E	σ, rel	C/E	σ, rel
127	SP	0.7980	0.0236	0.8457	0.1104	0.8013	0.0225
128	SH(BCNA)	0.8413	0.0147	0.9022	0.0407	0.8408	0.0133
129	SH(BCNA)	0.9015	0.0098	0.9601	0.0197	0.8797	0.0070
130	SH(BCNA)	0.9234	0.0106	0.9868	0.0150	0.9681	0.0041
131	RR(SSNA)	1.0055	0.0099	0.9494	0.0127	0.9597	0.0020
132	OC	1.0000	0.0112	1.0000	0.0104	1.0000	0.0100

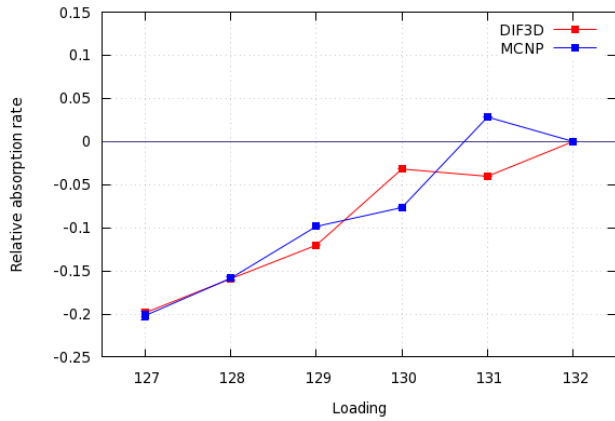


Fig. 7. Error of $^{10}\text{B}(n,\alpha)$ reaction rate

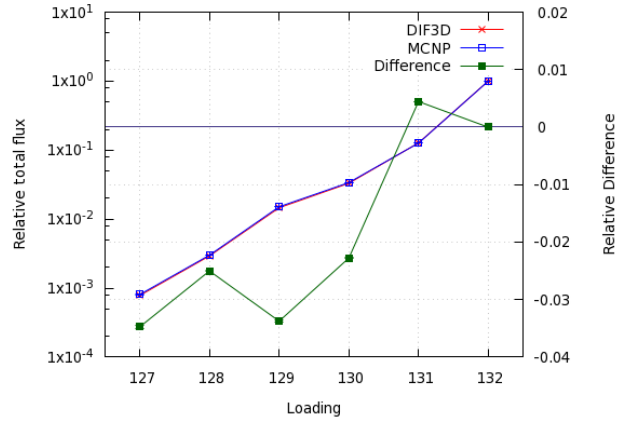
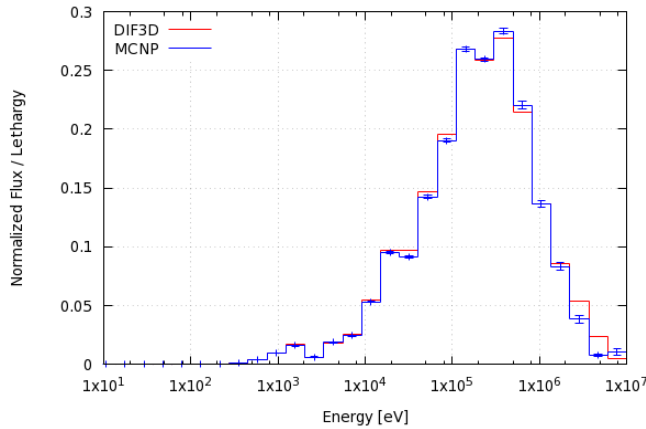
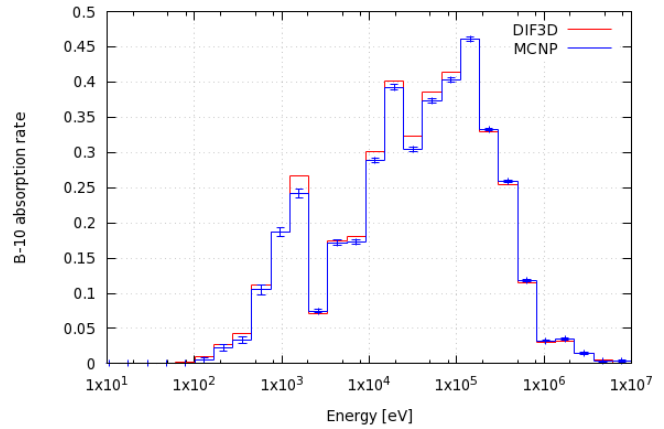


Fig. 8. Flux level between DIF3D and MCNP

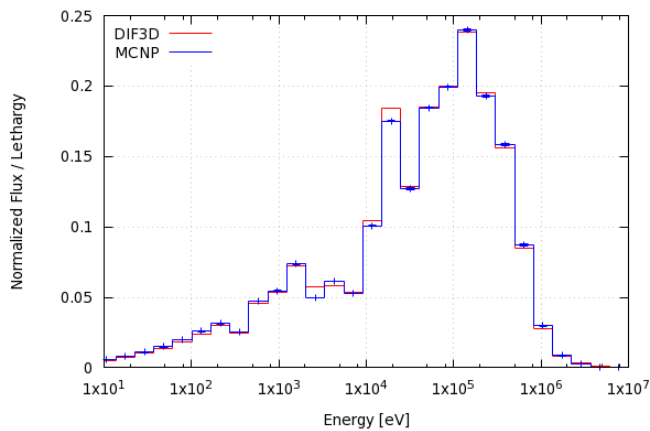


(a) Neutron spectrum

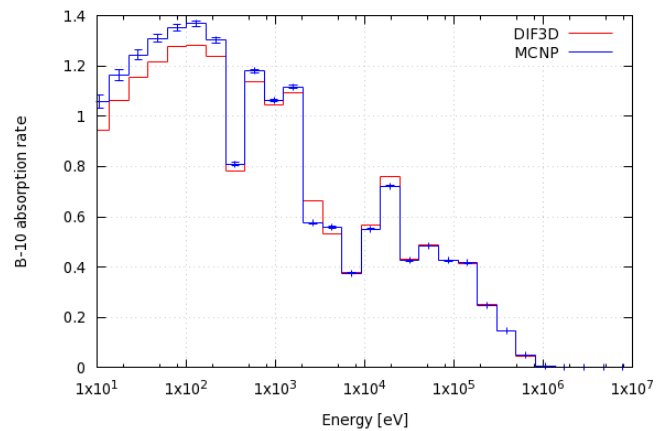


(b) $^{10}\text{B}(n,\alpha)$ reaction rate

Fig. 9. Neutron spectrum and $^{10}\text{B}(n,\alpha)$ reaction rate in core (L132)

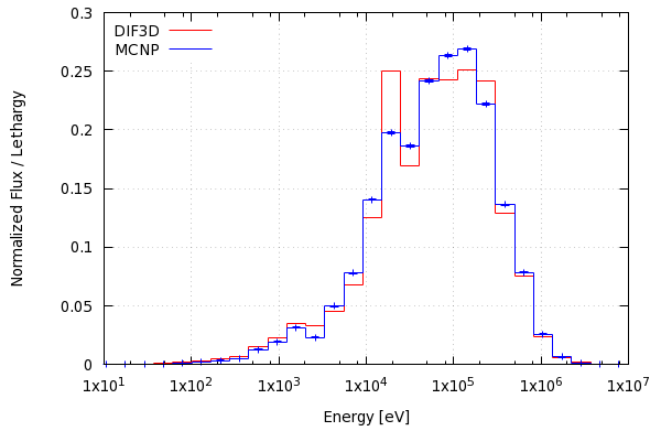


(a) Neutron spectrum

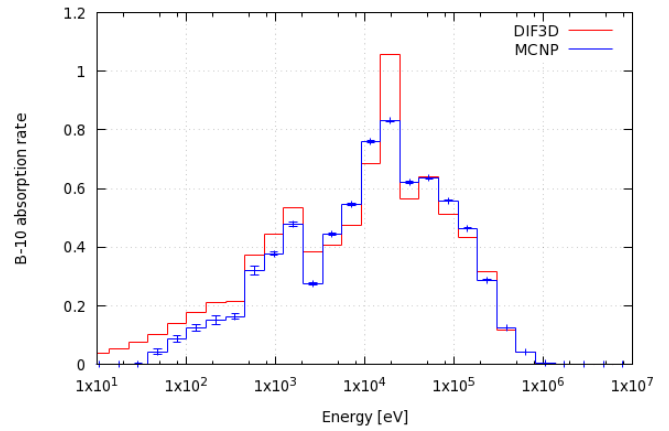


(b) $^{10}\text{B}(n,\alpha)$ reaction rate

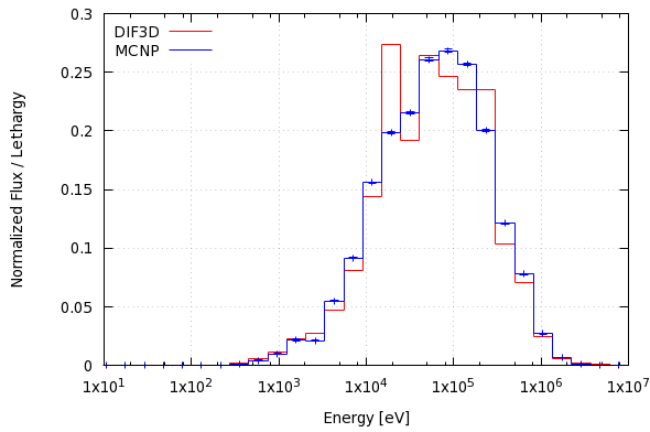
Fig. 10. Neutron spectrum and $^{10}\text{B}(n,\alpha)$ reaction rate in SSNA (L131)



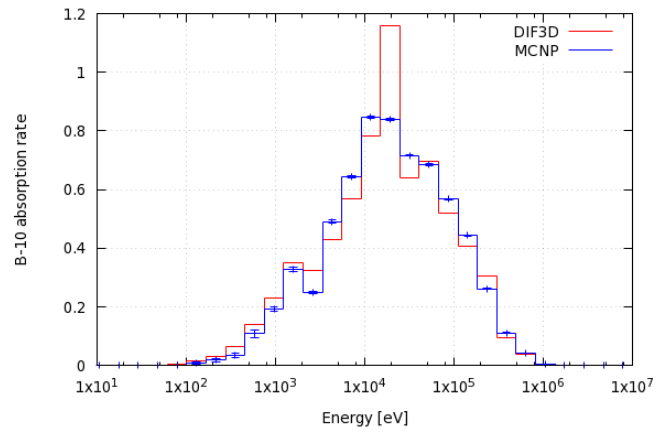
(a) Neutron spectrum in L130



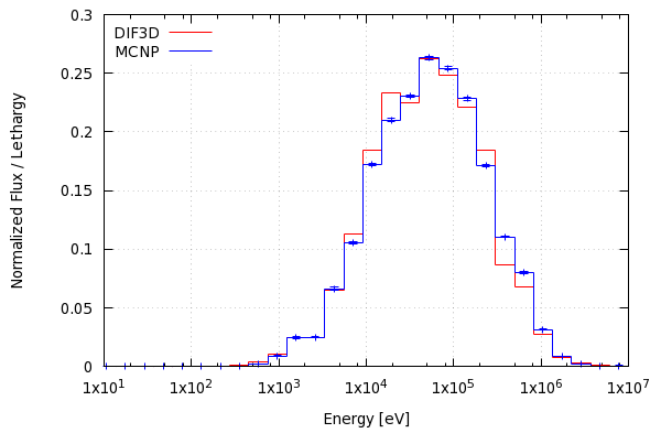
(b) $^{10}\text{B}(n,\alpha)$ reaction rate in L130



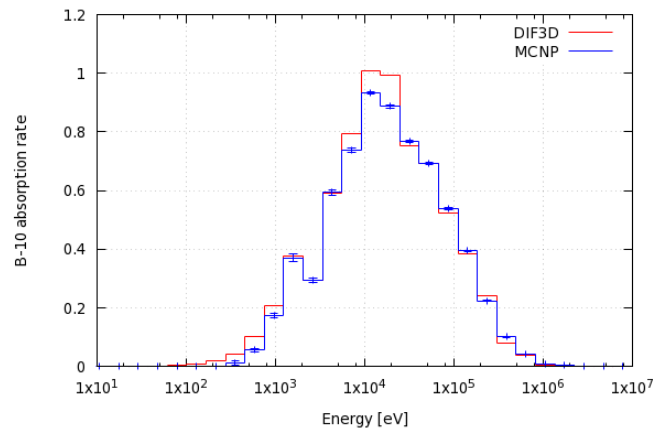
(c) Neutron spectrum in L129



(d) $^{10}\text{B}(n,\alpha)$ reaction rate in L129



(e) Neutron spectrum in L128



(f) $^{10}\text{B}(n,\alpha)$ reaction rate in L128

Fig. 11. Neutron spectrum and $^{10}\text{B}(n,\alpha)$ reaction rate in BCNA

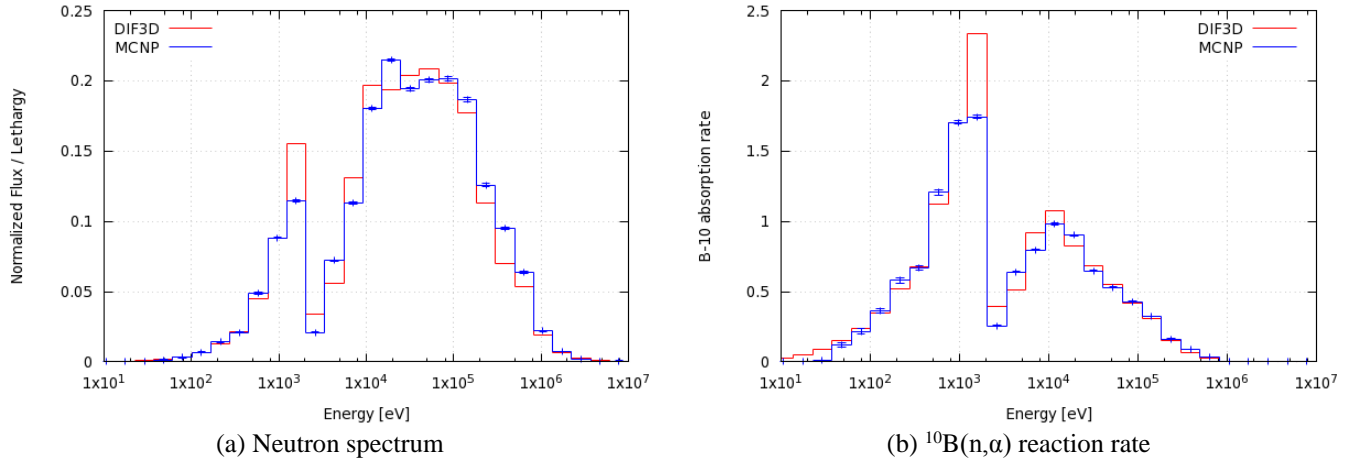


Fig. 12. Neutron spectrum and $^{10}\text{B}(n,\alpha)$ reaction rate in SP (L127)

The neutron spectrum and $^{10}\text{B}(n,\alpha)$ reaction rate are quite similar in outer core according to Fig. 9. The reaction rate as well as neutron spectrum matches greatly for outer core. Since the absorption rates are normalized by the value at outer core, the good agreement of neutron spectrum and reaction rate distribution gives a validity in estimating relative absorption rates in other regions. Meanwhile, minor difference was observed in higher energy regions when the neutron spectrum is compared, but not important in terms of reactor characteristics. The reaction rate of DIF3D was observed slightly greater below the Na-23 resonance compare to MCNP while the neutron flux is almost the same. This implies that the homogenized cross section of B-10 is slightly greater below the resonance of Na-23, 2.85keV.

Fig. 10 shows the important resonance of Fe-56 at 27.7keV obviously as a dip in neutron spectrum. The shapes of neutron spectra are very similar between DIF3D and MCNP, while slightly greater neutron flux level was observed in MCNP below the first Na-23 resonance. The difference becomes more significant for reaction rate since B-10 cross section is greater for lower energy regions.

Unlike outer core and SSNA, significantly different neutron spectrum was observed in BCNA, loading 130 and 131 as plotted in Fig. 11. The DIF3D neutron spectra in L130 and L129 look similar to L131 because of the existence of a dip around Fe-56 resonance. The dip was faded out in L128 which is away from SSNA. On the other hand, the flux dip by Fe-56 resonance were almost disappeared in MCNP results. This implies that the neutron spectrum after crossing the SSNA region becomes different between MCNP and DIF3D. Basically, the amount of absorbed neutrons during the slowing down is highly dependent on the resonance self-shielding. The methodologies of resonance treatment are significantly different between MCNP and MC²-3, the flux level below the Fe-56 resonance can be slightly different after SSNA regions. Another possible reason for the difference might be

the 0D homogenization of non-fuel drawers. Non-fuel drawers are also heterogeneous, but its heterogeneity might be insignificant in the core calculation. However, the spatial self-shielding effect becomes important around resonance energy regions. More neutrons will be absorbed by the resonance in homogeneous models than heterogeneous models.

For sodium pool, the neutron spectrum mismatches below the Na-23 resonance, which is similar to the phenomenon observed in L131 and L130. However, the absorbed neutron by the resonance is smaller in the deterministic model. Since the drawers in SP are almost homogeneous unlike the drawers in SSNA, the different resonance methodologies between deterministic models and stochastic model might cause the error around the resonance.

3. Examination on the effects of the TWODANT procedure

For a slowing down calculation, MC²-3 code requires neutrons sources. If the problem involves fissionable isotopes, their fission neutrons will be used as sources. If not, U-238's fission neutrons will be used. If the target homogenized region is fuel, the spectra of neutron sources will be fairly realistic. However, the target region does not have fissionable isotopes, the neutron spectrum in those regions will be softer than U-238 fission neutron's. Additionally, blanket regions have fissionable isotopes, but the majority of neutrons in that region is not generated from the fissions reactions of those isotopes; most of neutrons are coming from fuels after scattering. In these cases, realistic neutron spectrum is normally unknown without a core transport calculation. A TWODANT R-Z calculation is required to obtain approximated yet accurate neutron spectrum for each region. As mentioned previously, the spectrum obtained from TWODANT calculation will be used for group collapsing.

The effect of TWODANT R-Z model was simply examined by removing the first two procedures in Fig. 2. The $^{10}\text{B}(n,\alpha)$ reaction rate of two different procedures were compared in Fig. 12. Against our expectations, the maximum difference in relative reaction rate was observed about 1%, so the effect of TWODANT procedure turned out to be very minor in this analysis.

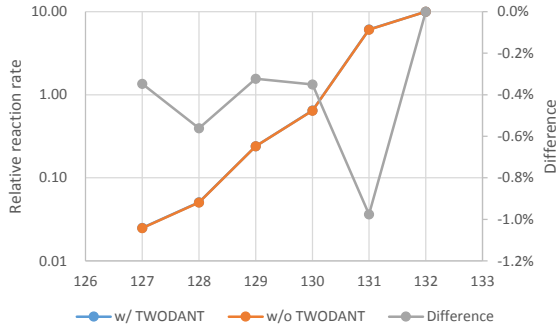


Fig. 12. The difference between two deterministic models

If the spectrum transition is severe such as blanket free cores, or if only few energy groups are used, consideration of realistic neutron spectrum becomes important in multi-group cross section generation. However, the ZPPR-15 cores have axial and radial blanket regions, so the spectrum transition at a region interface is insignificant and the effect of TWODANT procedure can be hardly seen. Also 33 energy group can be considered fine enough to analyze ZPPR-15 cores. Fig. 13 shows 33G $^{10}\text{B}(n,\alpha)$ reaction cross sections in various regions with TWODANT procedure, and similar multi-group cross sections are observed except for L132. This shows the spectrum used for group collapsing is less important in ZPPR-15.

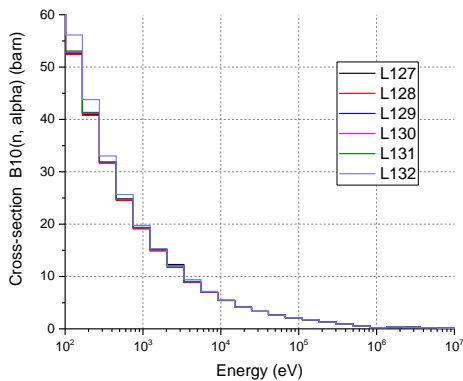


Fig. 13. 33G $^{10}\text{B}(n,\alpha)$ reaction cross sections

V. CONCLUSIONS

MC²-3/TWODANT/DIF3D models were successfully developed for ZPPR-15 $^{10}\text{B}(n,\alpha)$ reaction rate measurement

analysis. The multi-group cross sections are collapsed based on two different TWODANT R-Z models in order to account the asymmetric core configuration. Beside the measured data, reference solutions are generated from MCNP6 with weight window technique.

By comparing the MC²-3/TWODANT/DIF3D results with MCNP's and measured data, the decrement of $^{10}\text{B}(n,\alpha)$ along the radial position of reactor was observed similar between MC²-3/TWODANT/DIF3D and MCNP, and showed minor error compared to measured data. The maximum error was observed 20% at sodium pool, which is acceptable when the problem can be considered as a shielding problem. Compared to MCNP results, generally good agreement was observed in maximum error, the neutron spectrum, and the $^{10}\text{B}(n,\alpha)$ reaction rate. However, considerable discrepancies in neutron spectrum and $^{10}\text{B}(n,\alpha)$ reaction rate were observed in BCNA and SP area near Fe-56 and Na-23 resonances because of inaccurate spatial self-shielding in the deterministic models and the different resonance methodology between deterministic and stochastic approaches. The TWODANT procedure for more accurate multi-group cross section generation was turned out to be insignificant in problem, because the blanket areas can prevent severe spectrum transition.

ACKNOWLEDGMENTS

This work was supported by the U.S.-ROK I-NERI collaborative project: the Korea government (MSIP) funded the National Research Foundation of Korea (NRF) grant number NRF-2013M2A8A2078239 and the U.S. Department of Energy (DOE) under Contract number DE-AC02-06CH11357.

REFERENCES

1. H. F. MCFARLANE, et al., 'Benchmark Physics Tests in the Metallic-Fueled Assembly ZPPR-15,' *Nucl. Sci. Eng.*, 101, pp. 137 – 152 (1989).
2. C. H. LEE and W. S. YANG, "MC²-3: Multigroup Cross Section Generation Code for Fast Reactor Analysis," ANL/NE-11-41, Argonne National Laboratory, January (2012).
3. M. A. SMITH, E. E. LEWIS, and E. R. SHEMON, "DIF3D-VARIANT 11.0, A Decade of Updates," ANL/NE-14/1, Argonne National Laboratory (2014).
4. H. K. JOO, et al., "Status of the fast reactor technology development in Korea," The 48th TWG-FR Meeting, Obninsk, May 25–29 (2015).
5. D. PELOWITZ, "MCNP6 User's Manual Version 1.0", LA-CP-13-0064, Los Alamos National Laboratory (2013).
6. B.C. KIEDROWSKI, MCNP6 for Criticality Accident Alarm System, LA-UR-12-25545, Los Alamos National Laboratory (2012)